American Journal of Civil Engineering
2026, Vol. 14, No. 3, pp. 193–204
https://doi.org/10.11648/j.ajce.20261403.16

Research Article

Mechanical Properties and Chloride Penetration Resistance of Low-Carbon Concrete with Blended Binder Systems

Nam Wook Kim[1, *], **Seung Soo Ryu**[2]

[1]Department of Civil Engineering, Joongbu University, Goyang, Republic of Korea
[2]Soo Engineering Co., Cheonan, Republic of Korea

Abstract

The production of ordinary Portland cement (OPC) is associated with substantial CO_2 emissions, while reinforced concrete structures exposed to marine or deicing-salt environments require improved resistance to chloride-induced deterioration. Although supplementary cementitious materials (SCMs) and fine mineral powder (FMP) have been used to reduce cement consumption, further clarification is needed regarding how binder composition and curing condition jointly influence strength development, shrinkage, carbonation, chloride binding, and chloride transport. This study investigated the mechanical properties and chloride penetration resistance of low-carbon concrete with blended binder systems incorporating ground granulated blast-furnace slag (GGBS), fly ash (FA), silica fume (SF), and FMP. Concrete mixtures with design compressive strength levels of 30 and 45 MPa were prepared using OPC, GGBS, and FA binder systems with FMP substitution, and an 80 MPa ternary binder mixture containing FA and SF was also examined. The experimental program included compressive strength, flexural strength, splitting tensile strength, static modulus of elasticity, drying shrinkage, accelerated carbonation, salt-water immersion, water-soluble chloride, total chloride, chloride binding ratio, and apparent chloride diffusion coefficient evaluations. The results showed that FMP substitution increased compressive strength, reduced carbonation rate coefficients, increased chloride binding ratio, and decreased the apparent diffusion coefficient, particularly in blended binder systems. These findings indicate that optimized blended binder systems can contribute to low-carbon concrete with enhanced durability in chloride-bearing environments, provided that mechanical performance, dimensional stability, carbonation resistance, and chloride binding capacity are considered together.

Keywords

Low-carbon Concrete, Blended Binder Systems, Supplementary Cementitious Materials, Fine Mineral Powder, Chloride Penetration Resistance, Carbonation Resistance, Durability

*Correspondence: Nam Wook Kim (nwkim@joongbu.ac.kr)

Received: 21 May 2026; **Accepted:** 5 June 2026; **Published:** 29 June 2026

1. Introduction

Concrete is the most widely used construction material for social infrastructure, including buildings, bridges, ports, marine structures, and transportation facilities. However, the production of ordinary Portland cement (OPC), which is the main binder in concrete, is accompanied by a considerable environmental burden because CO_2 is emitted during limestone calcination and high-temperature clinker manufacturing. Reducing clinker content and increasing the use of supplementary materials are therefore important strategies for developing low-carbon and environmentally sustainable concrete [1, 2].

One effective approach to reducing the environmental impact of cement-based materials is the use of supplementary cementitious materials (SCMs) as partial replacements for cement. Industrial by-products and mineral admixtures such as ground granulated blast-furnace slag (GGBS), fly ash (FA), silica fume (SF), and fine mineral powder (FMP) can reduce cement consumption and contribute to resource recycling. These materials can also improve concrete performance through physical filler effects, pozzolanic reactions, and latent hydraulic reactions, depending on their chemical and mineralogical characteristics [3, 4].

In addition to environmental performance, the durability of concrete structures is a critical requirement for sustainable construction. Among various deterioration mechanisms, chloride-induced corrosion of reinforcing steel is one of the most serious durability problems in reinforced concrete structures exposed to marine environments, coastal areas, and deicing salts. Once chloride ions penetrate the concrete cover and reach the reinforcing steel at a critical concentration, the passive film on the steel surface may be destroyed, initiating corrosion and causing cracking, delamination, and spalling of the concrete cover [8, 9, 12, 15].

In coastal regions and mountainous areas where deicing agents are used, structures are required to have resistance to salt attack. Common countermeasures include the use of epoxy-coated reinforcing bars and increased concrete cover. However, these measures can increase member thickness and fabrication cost. Therefore, it is preferable to improve salt resistance by reducing chloride ingress through modification of the concrete material itself [5, 6, 10, 11].

Previous studies have shown that SCMs such as FA and GGBS can improve resistance to chloride penetration, while carbonation resistance and chloride binding behavior depend strongly on binder chemistry, pore refinement, curing, and exposure conditions [6, 7, 11, 19-24]. However, the combined influence of FMP substitution, blended binder type, and curing condition on mechanical properties, carbonation behavior, chloride binding ratio, and apparent chloride diffusion coefficient has not been sufficiently clarified. This research gap is particularly relevant for precast and low-carbon concrete products used in salt-damage countermeasure regions.

Based on these considerations, this study evaluates the mechanical properties and chloride ion penetration resistance of low-carbon concrete with blended binder systems. Particular attention is paid to the effects of SCMs, FMP substitution, and curing condition on strength development, drying shrinkage, carbonation resistance, chloride binding, and the apparent chloride diffusion coefficient. The results are intended to provide practical data for selecting binder systems that reduce cement consumption while maintaining durability in chloride-bearing environments.

2. Experimental Program

2.1. Materials and Mixture Proportions

Tables 1 to 3 show the properties of the materials used, the chemical composition of the admixtures, and the mixture proportions. The concrete mixtures were designed according to the target compressive strength level and binder system. For planned mixtures with design compressive strengths of 30 and 45 MPa, OPC mixtures and mixtures in which part of the cement was replaced by GGBS or FA were prepared. In addition, for each of these mixtures, a mixture in which 20 kg/m^3 of cement was replaced by FMP was prepared.

The amount of FMP replacement was fixed at 20 kg/m^3 for all applicable mixtures. Therefore, the relative replacement ratio became higher in mixtures with lower binder content. An 80 MPa ultra-high-strength mixture was also prepared to examine the influence of a dense matrix on chloride penetration resistance. This mixture did not contain FMP and was designed as a ternary binder system containing FA and SF. Figure 1 summarizes the principal materials and binder components used in the experimental program.

Table 1. *Materials used in this study.*

Material	Symbol	Density (g/cm^3)	F.M.
Ordinary Portland cement	OPC	3.16	-
Blast-furnace slag fine powder	GGBS	2.91	-
Fly ash, Type II	FA	2.28	-

Material	Symbol	Density (g/cm^3)	F.M.
Silica fume	SF	2.25	-
Fine mineral powder	FMP	2.37	-
Sea sand	S	2.57	2.51
Crushed stone	CA	2.92	6.60
High-range water-reducing admixture	HRWRA	1.05	-

Table 2. Chemical composition of mineral admixtures (mass%).

Material	SiO_2	Al_2O_3	Fe_2O_3	CaO
GGBS	27.9	11.6	0.27	39.3
FA	49.4	18.1	4.03	2.51
SF	84.4	0.51	0.52	0.18
FMP	57.9	29.2	0.63	0.06

Table 3. Mixture proportions used in this study.

Fc (MPa)	Mixture ID	W/B (%)	s/a	W	C	GGBS	FA	SF	FMP	S	CA	SL/Sf (cm)	Air (%)	C.T. (℃)	Cl- (kg/m^3)
30	C30-OPC	48	41.3	165	324	-	-	-	20	748	1206	9.5	1.9	29.0	0.076
30	C30-GGBS	46	40.7	165	231	108	-	-	20	728	1206	11.0	1.0	30.0	0.083
30	C30-FA	40	38.2	165	297	-	100	-	20	657	1206	12.5	1.8	26.0	0.065
45	C45-OPC	37	38.5	165	426	-	-	-	20	665	1206	12.5	1.1	26.0	0.080
45	C45-GGBS	35	37.4	165	310	141	-	-	20	634	1206	13.0	1.7	25.0	0.064
45	C45-FA	32	35.2	165	396	-	100	-	20	577	1206	14.5	1.6	25.0	0.030
80	C80-FA-SF	25	44.9	150	450	-	90	60	-	724	1008	65.5	1.2	30.0	0.032

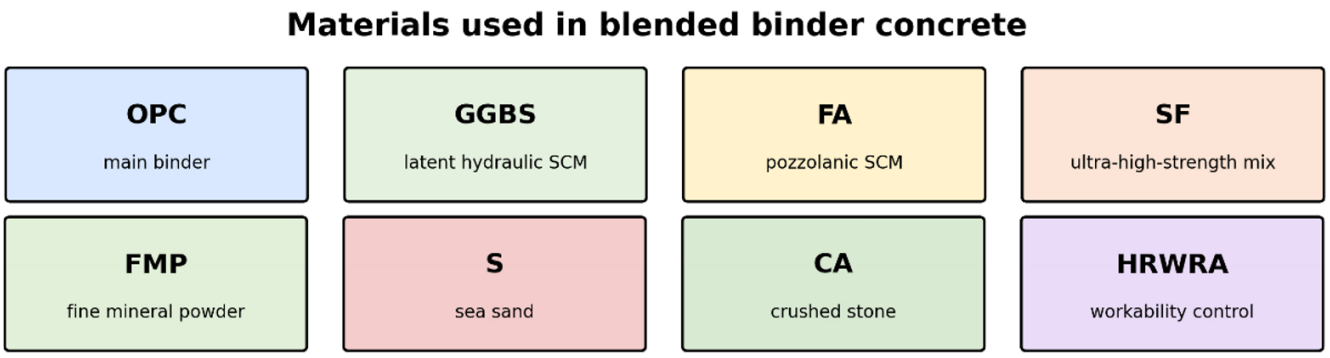

Figure 1. Materials and binder components used in this study.

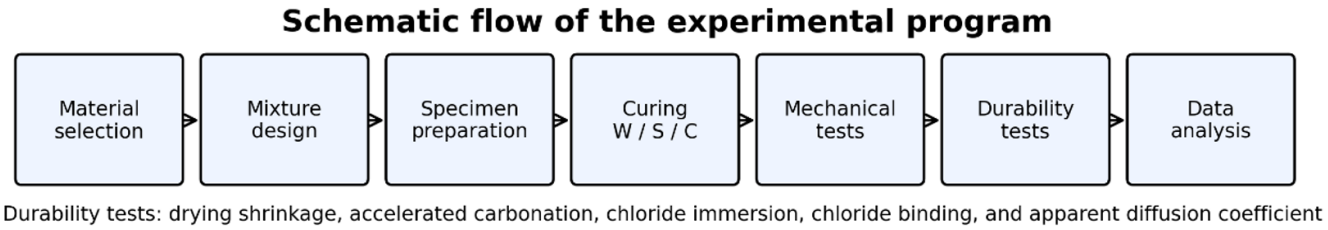

Figure 2. *Schematic flow of the experimental program.*

2.2. Experimental Methods

Table 4 lists the test types and test methods, and Figure 2 summarizes the experimental workflow. Cylindrical specimens 100 mm in diameter and 200 mm in height were used for compressive strength, Young's modulus, and splitting tensile strength tests. Prismatic specimens measuring 100 x 100 x 400 mm were used for flexural strength tests. The test method descriptions were reorganized using ASTM and EN standards where technically applicable, while retaining the original experimental conditions [16-18].

Table 4. *Test items and test methods.*

Category	Test item	Test method
Mechanical properties	Compressive strength	ASTM C39/C39M
	Flexural strength	ASTM C78/C78M
	Splitting tensile strength	ASTM C496/C496M
	Static modulus of elasticity	ASTM C469/C469M
Durability	Drying shrinkage	ASTM C157/C157M
	Accelerated carbonation	EN 12390-12:2020
	Apparent diffusion coefficient of chloride ion	ASTM C1556
	Water-soluble chloride content	ASTM C1218/C1218M
	Acid-soluble chloride content / total chloride content	ASTM C1152/C1152M

Specimen curing was based on standard curing (W) and steam curing (S). Only for the ultra-high-strength mixture, constant-temperature and constant-humidity curing (C) was used instead of steam curing. W indicates that specimens were kept in air at the casting site until one day after casting and then cured in water at 20±2°C after demolding. S indicates steam curing under the same conditions as precast concrete members, consisting of a pre-curing period of 2 h, a heating rate of 20°C/h, holding at a maximum temperature of 65°C for 1 h, and subsequent gradual cooling. After steam curing, specimens were stored in a constant-temperature and constant-humidity room at 20°C and 60% relative humidity until testing. C indicates curing in a constant-temperature and constant-humidity room at 20°C and 60% relative humidity from immediately after casting until the specified test age. [16-18]

Drying shrinkage was measured by the dial-gauge method using gauge plugs embedded in prismatic specimens. For standard-cured specimens, the initial length was measured after 7 days of standard curing, followed by secondary curing. For steam-cured specimens, the same steam curing condition as that used for precast concrete members was applied, and the initial length was measured at an age of 7 days. Drying shrinkage strain was measured for up to 26 weeks. [16]

The accelerated carbonation test was conducted under a carbon dioxide concentration of 5% for up to 26 weeks. Specimens used for drying shrinkage were reused for the carbonation test after curing in a constant-temperature and constant-humidity room. For international presentation, the carbonation test was described with reference to EN 12390-12:2020 because the original exposure conditions were retained. The results were therefore used as comparative indicators of carbonation resistance among mixtures rather than direct service-life prediction values. [18, 19]

The salt-water immersion test was conducted by processing cylindrical specimens and immersing them in a 10% NaCl aqueous solution for 2 years. After immersion, specimens were cut into five layers at 15 mm intervals in the depth direction, and soluble chloride content and total chloride content

were measured for each layer. Soluble chloride content was measured by dissolving the powdered sample in purified water at 50 ℃ and using the electrode-current method, while total chloride content was measured by the silver nitrate titration method. The apparent diffusion coefficient was calculated by regression analysis using the solution of Fick's diffusion equation, with reference to the concept of bulk diffusion testing in ASTM C1556 [17, 20-24].

3. Results and Discussion

3.1. Strength Test Results

Tables 5 and 6 show the results of the strength tests, and Figures 3 and 4 show the increase in compressive strength due to replacement with FMP. Compared with previous results without FMP, the use of FMP increased compressive strength by an average of approximately 40% up to the age of 28 days. The increase was more remarkable for steam-cured specimens than for standard-cured specimens. This indicates that the effects of FMP substitution are strongly related to early-age hydration and curing temperature. Similar strength enhancement trends in blended or particle-modified binder systems have been associated with filler effects, improved packing, and secondary hydration products [3, 4, 13, 14].

Although scatter was observed in the measurements of flexural strength, splitting tensile strength, and Young's modulus, these values tended to improve when FMP was used. This tendency is thought to be related to the microfiller effect of the fine powder, which has a fineness exceeding 10 m^2/g, and to pozzolanic reaction associated with the unhydrated SiO_2 and Al_2O_3 contained in the powder. These effects are considered to promote densification of the concrete matrix and improvement of the interfacial transition zone. The interpretation is consistent with the role of SCMs and fine powders in modifying the interfacial transition zone and pore structure [3, 4].

Table 5. *Strength test results for the 30 MPa series.*

Type	Property	Value at 1 d	Value at 14 d	Value at 28 d	Increase at 1 d (%)	Increase at 14 d (%)	Increase at 28 d (%)
C30-OPC-W	fc	-	53.4	61.1	-	33.6	38.2
C30-OPC-W	fb	-	6.00	7.17	-	10.6	11.6
C30-OPC-W	fst	-	3.73	4.69	-	6.7	35.3
C30-OPC-W	Ec	-	39.9	44.4	-	12.8	21.6
C30-OPC-S	fc	24.7	49.1	55.2	40.2	43.1	53.2
C30-OPC-S	fb	-	5.47	4.96	-	55.4	4.8
C30-OPC-S	fst	-	3.86	3.73	-	44.0	11.3
C30-OPC-S	Ec	-	38.0	41.4	-	23.1	26.6
C30-GGBS-W	fc	-	62.4	70.6	-	33.3	35.0
C30-GGBS-W	fb	-	7.27	8.17	-	22.3	34.8
C30-GGBS-W	fst	-	4.16	5.00	-	15.2	28.1
C30-GGBS-W	Ec	-	42.5	44.3	-	18.1	16.1
C30-GGBS-S	fc	25.2	57.1	60.7	55.8	58.3	61.5
C30-GGBS-S	fb	-	4.53	5.33	-	22.7	24.8
C30-GGBS-S	fst	-	3.70	4.10	-	37.4	42.0
C30-GGBS-S	Ec	-	42.1	38.2	-	34.8	19.6
C30-FA-W	fc	-	58.1	66.1	-	32.1	33.3
C30-FA-W	fb	-	6.51	7.11	-	14.9	25.3
C30-FA-W	fst	-	4.25	4.79	-	46.2	48.7
C30-FA-W	Ec	-	41.9	45.8	-	9.3	18.3
C30-FA-S	fc	27.1	52.5	55.9	33.0	38.8	39.3
C30-FA-S	fb	-	4.45	4.68	-	7.6	9.5

Type	Property	Value at 1 d	Value at 14 d	Value at 28 d	Increase at 1 d (%)	Increase at 14 d (%)	Increase at 28 d (%)
C30-FA-S	fst	-	3.45	4.03	-	23.3	41.8
C30-FA-S	Ec	-	36.5	36.7	-	10.5	7.6
C80-FA-SF-W	fc	-	95.6	116	-	-	-
C80-FA-SF-W	Ec	-	47.7	49.5	-	-	-

Note: fc = compressive strength (MPa); fb = flexural strength (MPa); fst = splitting tensile strength (MPa); Ec = Young's modulus (GPa).

Table 6. *Strength test results for the 45 MPa series.*

Type	Property	Value at 1 d	Value at 14 d	Value at 28 d	Increase at 1 d (%)	Increase at 14 d (%)	Increase at 28 d (%)
C45-OPC-W	fc	-	70.5	77.5	-	33.1	34.5
C45-OPC-W	fb	-	7.03	8.35	-	16.4	22.6
C45-OPC-W	fst	-	4.29	4.80	-	17.4	20.1
C45-OPC-W	Ec	-	43.6	45.1	-	7.4	6.6
C45-OPC-S	fc	34.9	62.4	69.4	40.0	43.2	40.7
C45-OPC-S	fb	-	5.03	5.20	-	13.0	9.6
C45-OPC-S	fst	-	4.08	4.28	-	29.4	31.0
C45-OPC-S	Ec	-	42.1	42.3	-	17.7	6.1
C45-GGBS-W	fc	-	78.1	83.5	-	18.7	20.2
C45-GGBS-W	fb	-	8.93	9.69	-	22.9	23.2
C45-GGBS-W	fst	-	4.90	5.61	-	12.5	12.7
C45-GGBS-W	Ec	-	44.1	45.7	-	3.2	2.4
C45-GGBS-S	fc	34.6	71.4	75.5	28.1	35.5	31.2
C45-GGBS-S	fb	-	5.26	4.96	-	15.3	-7.1
C45-GGBS-S	fst	-	4.28	4.45	-	18.5	18.8
C45-GGBS-S	Ec	-	41.2	41.4	-	12.3	5.6
C45-FA-W	fc	-	68.9	76.8	-	22.5	19.2
C45-FA-W	fb	-	7.17	8.67	-	39.4	21.3
C45-FA-W	fst	-	4.68	4.91	-	28.8	23.7
C45-FA-W	Ec	-	45.2	44.7	-	20.0	8.2
C45-FA-S	fc	36.1	60.2	66.1	40.6	26.7	28.3
C45-FA-S	fb	-	4.33	4.50	-	-0.7	-9.6
C45-FA-S	fst	-	3.78	4.39	-	19.2	18.1
C45-FA-S	Ec	-	43.4	39.8	-	20.8	7.9
C80-FA-SF-C	fc	31.1	101	105	-	-	-
C80-FA-SF-C	Ec	-	46.2	48.4	-	-	-

Note: fc = compressive strength (MPa); fb = flexural strength (MPa); fst = splitting tensile strength (MPa); Ec = Young's modulus (GPa).

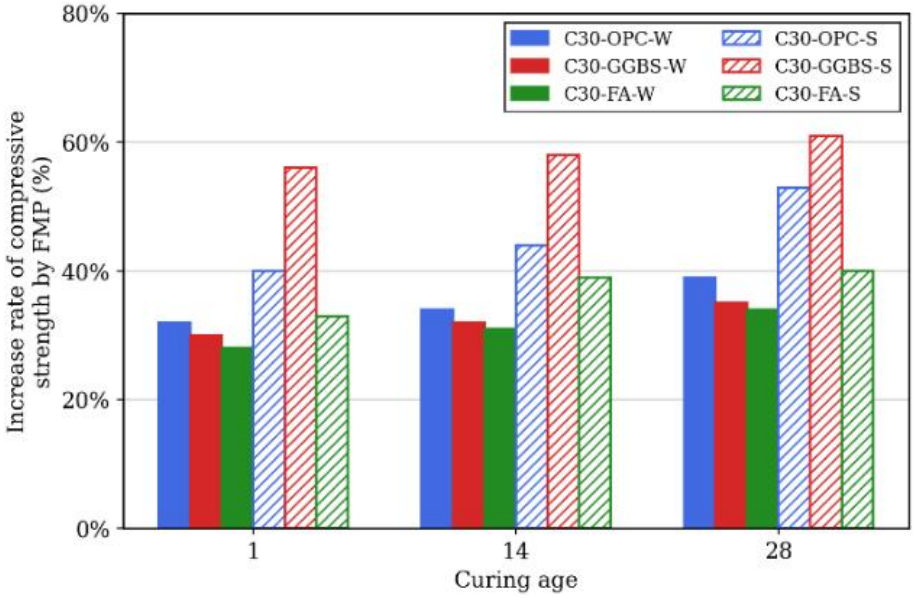

Figure 3. Increase rate of compressive strength by FMP for C30 mixtures.

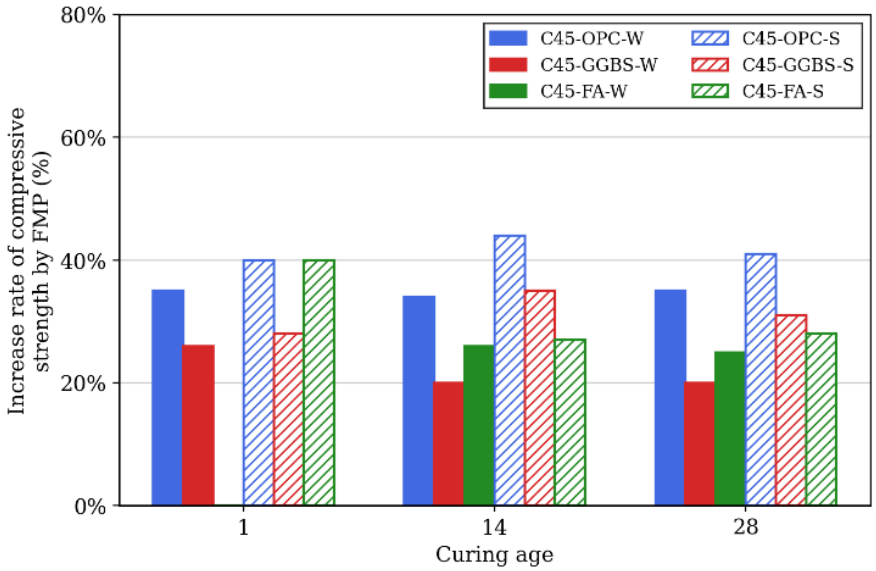

Figure 4. Increase rate of compressive strength by FMP for C45 mixtures.

3.2. Drying Shrinkage Strain

Figures 5 and 6 show the measured drying shrinkage strain for mixtures with and without FMP substitution. The plotted points represent measurements up to 26 weeks. The test results show that replacement with FMP reduced drying shrinkage strain for both standard-cured and steam-cured specimens. This effect is attributed to densification of the cement paste matrix and improvement of particle packing caused by the fine powder. Drying shrinkage behavior is influenced by binder chemistry, paste volume, pore refinement, and internal moisture movement [3, 13, 14].

For the 30 MPa mixtures, drying shrinkage tended to be reduced when FMP was used, and the reduction effect was observed over the measured period. For the 45 MPa mixtures, the influence of FMP was smaller than that for the 30 MPa mixtures, and the effect varied depending on binder type and curing condition. In mixtures containing FA, the reduction effect was relatively small compared with OPC and GGBS mixtures. This suggests that the effect of FMP on drying shrinkage depends on the original binder system, the degree of reaction of SCMs, and the curing history.

Because the reaction of FMP is considered to proceed mainly at early ages, steam curing may promote the densification effect more effectively than standard curing. However, excessive pore refinement can also influence moisture move-

ment and capillary stress. Therefore, the effect of FMP on drying shrinkage should be considered together with binder type, water-to-binder ratio, and curing condition.

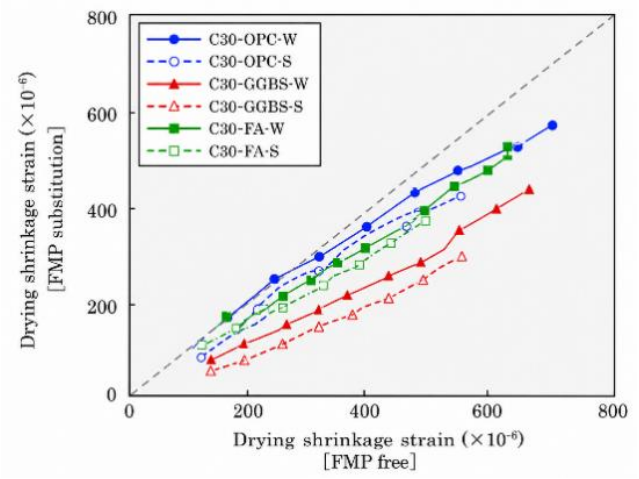

Figure 5. *Relationship between drying shrinkage strain of FMP-free and FMP-substituted C30 mixtures.*

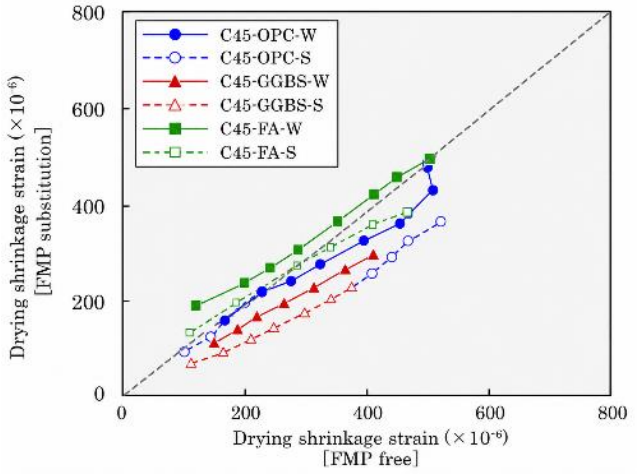

Figure 6. *Relationship between drying shrinkage strain of FMP-free and FMP-substituted C45 mixtures.*

3.3. Accelerated Carbonation Test Results

Figures 7 and 8 show the carbonation depth obtained from the accelerated carbonation test, and Figure 9 shows the carbonation rate coefficient. The exposure periods indicated in Figures 7 and 8 were converted considering that a carbon dioxide concentration of 5% in the accelerated carbonation test corresponds to approximately 100 times the carbon dioxide concentration in the atmosphere. Accordingly, the exposure period was expressed as an equivalent age in years for comparison of carbonation resistance. Carbonation behavior of blended binders must be interpreted together with pore transport properties and chemical buffering capacity [6, 11, 18, 19].

The results indicate that, in all mixtures in which FMP was used, the carbonation rate coefficient decreased. FMP has two opposing effects: a pozzolanic reaction that consumes calcium hydroxide and may promote carbonation, and a microfiller effect that densifies the pore structure and suppresses CO_2 ingress. In this study, the reduction in the carbonation rate coefficient suggests that the microfiller effect and resulting densification of the matrix had a dominant influence under the present test conditions.

The effect of FMP on carbonation resistance differed depending on binder type and curing condition. In blended binder systems, GGBS and FA can refine the pore structure through latent hydraulic and pozzolanic reactions, but these reactions can also reduce the calcium hydroxide content that provides alkalinity. Therefore, carbonation resistance should be interpreted by considering both physical transport resistance and chemical buffering capacity. The results also indicate that sufficient curing is important for developing carbonation resistance in mixtures containing SCMs and FMP.

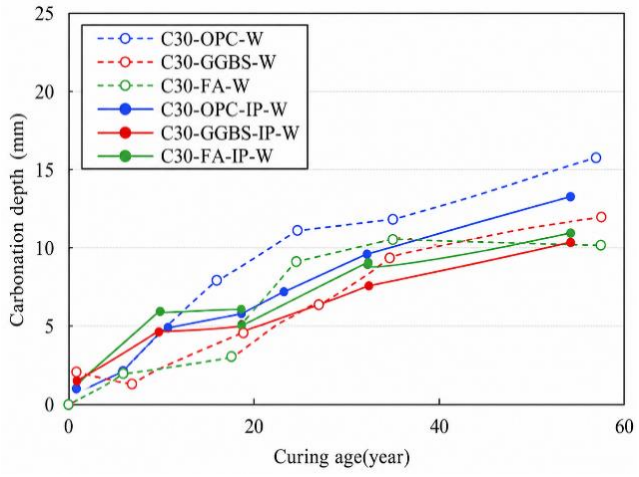

Figure 7. *Carbonation depth of C30 mixtures under standard curing.*

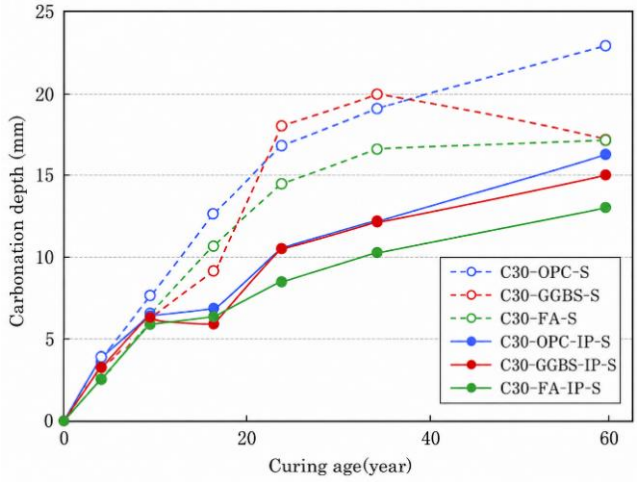

Figure 8. *Carbonation depth of C30 mixtures under steam curing.*

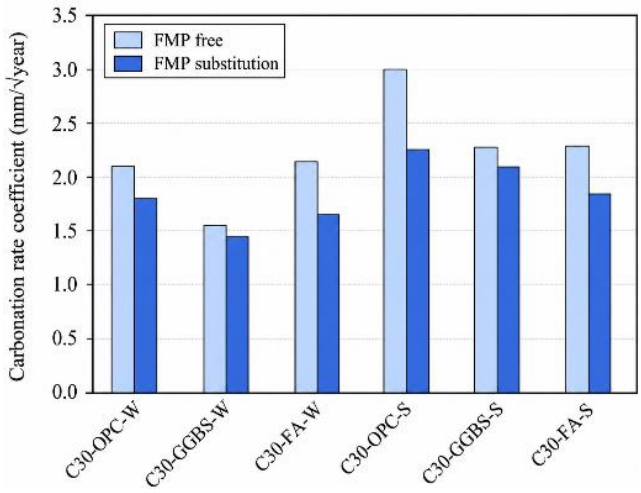

Figure 9. *Carbonation rate coefficient of C30 mixtures with and without FMP substitution.*

3.4. Chloride Penetration Test Results

Figures 10-13 show the measured chloride penetration amount, and Figures 14 and 15 show the relationship between the apparent diffusion coefficient and the chloride binding ratio. In Figures 10-13, legend symbols ending in A indicate results obtained by the electrode-current method, while those ending in B indicate results obtained by the silver nitrate titration method. The silver nitrate titration method was applied up to the third layer, where chloride penetration was clearly observed, corresponding to a depth of approximately 45 mm.

The chloride binding ratio was calculated using Eq. (1). In this study, the fixed chloride content was defined as the difference between the cumulative total chloride content measured up to the third layer by the silver nitrate titration method and the cumulative soluble chloride content measured by the electrode-current method. The chloride binding ratio was then calculated as the ratio of fixed chloride content to total chloride content.

$$\alpha_{fixed} = \frac{C_{tot} - C_{sol}}{C_{tot}} \times 100 \quad (1)$$

where α_{fixed} is the chloride binding ratio (%), C_{tot} is the total chloride content (kg/m^3), and C_{sol} is the water-soluble chloride content (kg/m^3).

The test results show that the chloride binding ratio was approximately 20-40% for mixtures without FMP substitution, whereas it increased to approximately 80% for FMP-substituted mixtures, more than doubling the value. This is considered to be due to the formation of Friedel's salt by unhydrated Al_2O_3 contained in FMP and adsorption in the densified microstructure caused by the microfiller effect. However, in the replacement mixtures, if the reaction of unhydrated C_3A proceeds during the early material age, it cannot be determined from this study whether the formation of Friedel's salt is greater than that in non-replacement mixtures. This issue remains for future investigation. In the ultra-high-strength mixture, the chloride binding ratio was also approximately 80%; however, because silica fume contains little Al_2O_3, adsorption to the fine pore structure is considered to account for most of the chloride fixation.

Figures 16 and 17 show the apparent diffusion coefficients of mixtures in which FMP was used. As shown in Figures 14 and 15, the apparent diffusion coefficient decreased at all strength levels when FMP was used, confirming the usefulness of FMP. The reduction effect of FMP on the apparent diffusion coefficient was most pronounced in the OPC mixture. As shown in Figures 16 and 17, when FMP was used in the FA and GGBS mixtures, the apparent diffusion coefficient was approximately half that of the OPC mixture. Even in mixed binder systems, FMP was confirmed to be effective. However, no clear difference due to curing method was observed. The influence of the salt-water immersion period on the apparent diffusion coefficient remains a subject for future study.

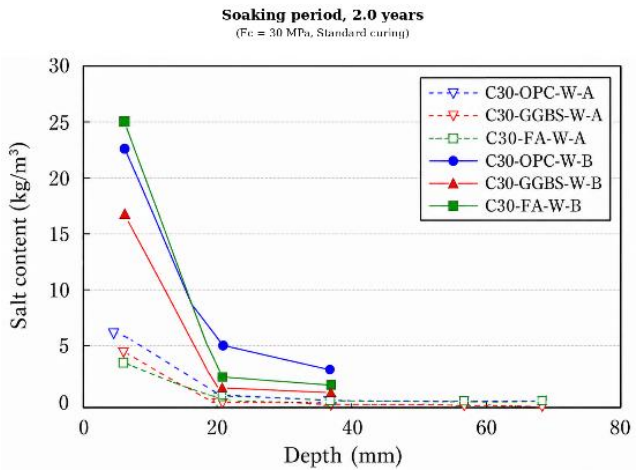

Figure 10. *Salt content profile after 2.0-year soaking for C30 mixtures under standard curing.*

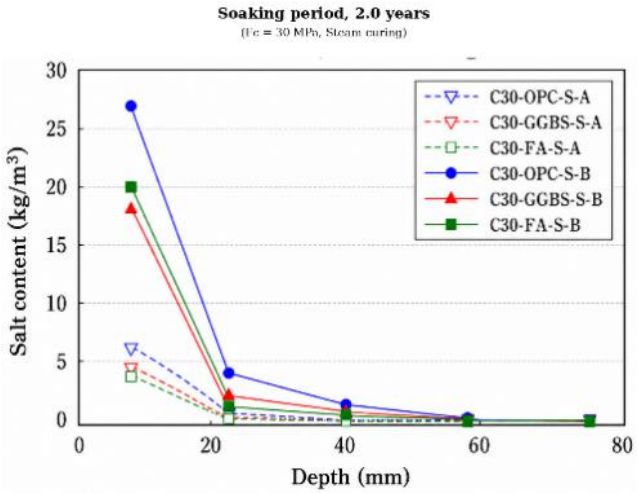

Figure 11. *Salt content profile after 2.0-year soaking for C30 mixtures under steam curing.*

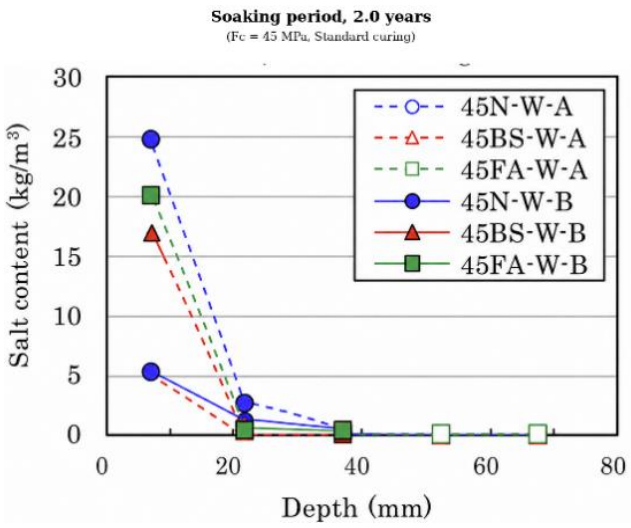

Figure 12. *Salt content profile after 2.0-year soaking for C45 mixtures under standard curing.*

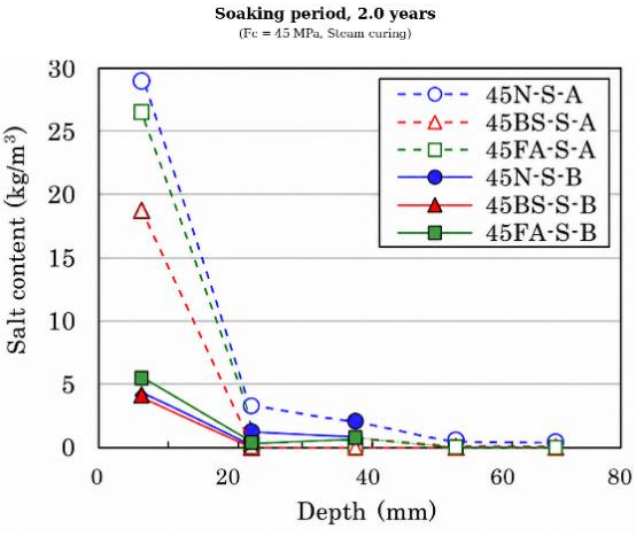

Figure 13. *Salt content profile after 2.0-year soaking for C45 mixtures under steam curing.*

3.5. Relationship Between Chloride Binding Ratio and Apparent Diffusion Coefficient

The relationship between the chloride binding ratio and apparent diffusion coefficient indicates that chloride binding capacity is closely related to chloride transport resistance. FMP-substituted mixtures tended to show both higher chloride binding ratios and lower apparent diffusion coefficients than FMP-free mixtures. This suggests that the improvement in chloride penetration resistance is caused not only by physical densification of the pore structure but also by chemical and physicochemical fixation of chloride ions. Recent studies have emphasized that chloride binding in blended binder systems involves both chemical reactions and physical sorption, and that these mechanisms should be considered with transport properties [7, 20-24].

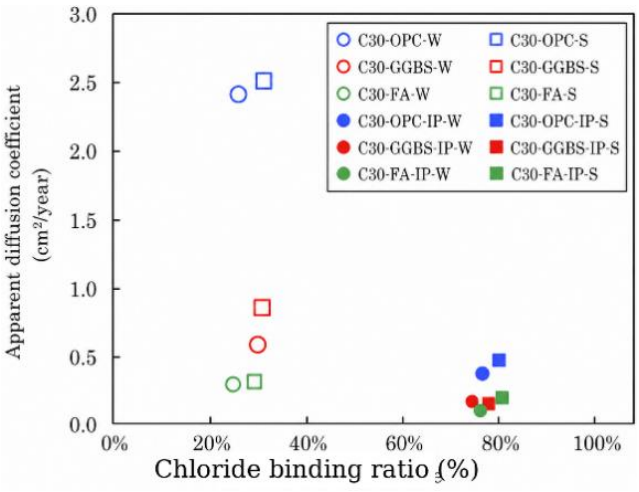

Figure 14. *Relationship between chloride binding ratio and apparent diffusion coefficient for C30 mixtures.*

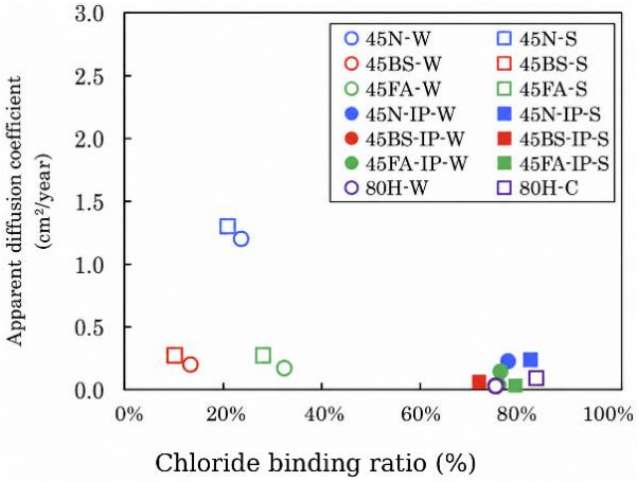

Figure 15. *Relationship between chloride binding ratio and apparent diffusion coefficient for C45 mixtures.*

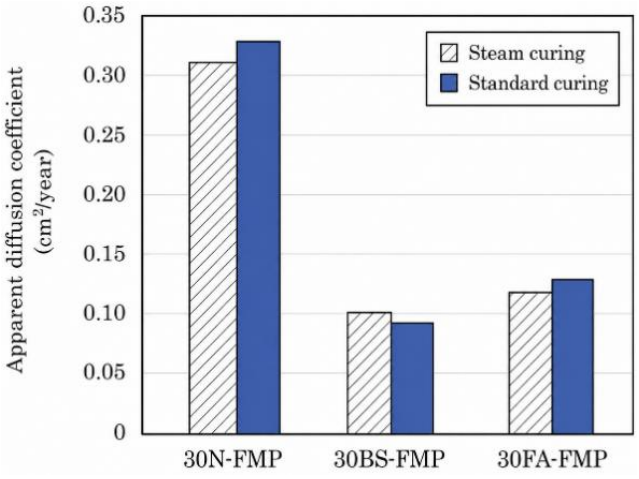

Figure 16. *Apparent diffusion coefficient of C30 FMP mixtures according to curing condition.*

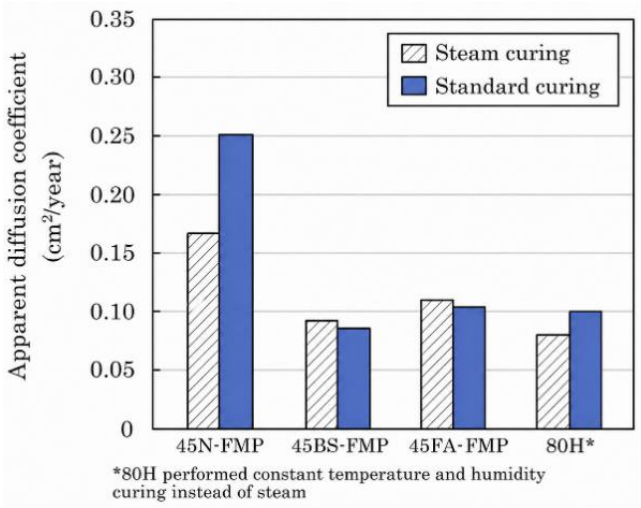

Figure 17. *Apparent diffusion coefficient of C45 FMP and 80H mixtures according to curing condition.*

Total chloride content includes both free and bound chloride, whereas water-soluble chloride content is more closely related to free chloride ions. Therefore, the comparison between total chloride content and water-soluble chloride content is useful for evaluating chloride binding behavior and the risk of reinforcement corrosion. The results demonstrate that blended binder systems incorporating FMP can improve chloride resistance by combining pore refinement with chloride fixation.

4. Conclusions

This study examined the applicability of low-carbon concrete with blended binder systems by evaluating mechanical performance, drying shrinkage, carbonation behavior, and chloride penetration resistance. The following conclusions summarize the effects of SCMs, FMP substitution, and curing conditions on the main performance indicators.

1) The use of supplementary cementitious materials, such as GGBS and FA, can reduce OPC consumption and contribute to the development of environmentally conscious concrete. Although these materials may delay early-age strength development, their latent hydraulic and pozzolanic reactions can improve later-age strength and microstructural densification under appropriate curing conditions.
2) FMP influenced mechanical properties and volume stability through filler effects, particle packing improvement, and possible pozzolanic reaction. Because its high fineness may affect moisture movement and drying shrinkage, the replacement level should be carefully controlled to achieve balanced strength development and dimensional stability.
3) The carbonation resistance of blended binder concrete was governed by both pore structure and chemical alkalinity. Mineral admixtures and FMP can densify the matrix and reduce CO_2 transport pathways, but they may also reduce calcium hydroxide content through pozzolanic or latent hydraulic reactions. Therefore, carbonation resistance should be evaluated by considering both physical densification and chemical buffering capacity.
4) Chloride ion penetration resistance was improved by the use of mineral admixtures and FMP. This improvement is mainly attributed to pore structure refinement, reduced connectivity of capillary pores, and enhanced chloride binding capacity. These results indicate that properly designed blended binder systems can contribute to low-carbon concrete with improved durability in chloride-bearing environments.

Author Contributions

Nam Wook Kim: Conceptualization, Investigation, Formal analysis, Methodology, Supervision, Project administration, Writing – original draft, Writing – review & editing

Seung Soo Ryu: Resources, Data curation, Investigation, Validation, Visualization, Writing – review & editing

Conflicts of Interest

The authors declare no conflicts of interest.

References

[1] Scrivener, K. L., John, V. M., and Gartner, E. M., Eco-efficient cements: Potential economically viable solutions for a low-CO_2 cement-based materials industry, Cement and Concrete Research, Vol. 114, pp. 2-26, 2018. https://doi.org/10.1016/j.cemconres.2018.03.015

[2] Flower, D. J. M., and Sanjayan, J. G., Greenhouse gas emissions due to concrete manufacture, The International Journal of Life Cycle Assessment, Vol. 12, No. 5, pp. 282-288, 2007. https://doi.org/10.1065/lca2007.05.327

[3] Lothenbach, B., Scrivener, K., and Hooton, R. D., Supplementary cementitious materials, Cement and Concrete Research, Vol. 41, No. 12, pp. 1244-1256, 2011. https://doi.org/10.1016/j.cemconres.2010.12.001

[4] Bentz, D. P., Ferraris, C. F., Jones, S. Z., Lootens, D., and Zunino, F., Limestone and silica powder replacements for cement: Early-age performance, Cement and Concrete Composites, Vol. 78, pp. 43-56, 2017. https://doi.org/10.1016/j.cemconcomp.2017.01.001

[5] Thomas, M. D. A., and Bamforth, P. B., Modelling chloride diffusion in concrete: Effect of fly ash and slag, Cement and Concrete Research, Vol. 29, No. 4, pp. 487-495, 1999. https://doi.org/10.1016/S0008-8846(98)00192-6

[6] Papadakis, V. G., Effect of supplementary cementing materials on concrete resistance against carbonation and chloride ingress, Cement and Concrete Research, Vol. 30, No. 2, pp. 291-299, 2000. https://doi.org/10.1016/S0008-8846(99)00249-5

[7] Thomas, M. D. A., Hooton, R. D., Scott, A., and Zibara, H., The effect of supplementary cementitious materials on chloride binding in hardened cement paste, Cement and Concrete Research, Vol. 42, No. 1, pp. 1-7, 2012. https://doi.org/10.1016/j.cemconres.2011.01.001

[8] Zhang, T., and Gjørv, O. E., Diffusion behavior of chloride ions in concrete, Cement and Concrete Research, Vol. 26, No. 6, pp. 907-917, 1996. https://doi.org/10.1016/0008-8846(96)00069-5

[9] Glass, G. K., and Buenfeld, N. R., The presentation of the chloride threshold level for corrosion of steel in concrete, Corrosion Science, Vol. 39, No. 5, pp. 1001-1013, 1997. https://doi.org/10.1016/S0010-938X(97)00009-7

[10] Sanjuán, M. Á., Estévez, E., Argiz, C., and del Barrio, D., Chloride diffusion in concrete made with coal fly ash, ternary and ground granulated blast-furnace slag Portland cements, Materials, Vol. 15, No. 24, Article 8914, 2022. https://doi.org/10.3390/ma15248914

[11] von Greve-Dierfeld, S., Lothenbach, B., Vollpracht, A., et al., Understanding the carbonation of concrete with supplementary cementitious materials: A critical review by RILEM TC 281-CCC, Materials and Structures, Vol. 53, Article 136, 2020. https://doi.org/10.1617/s11527-020-01558-w

[12] Gjørv, O. E., Durability Design of Concrete Structures in Severe Environments, 2nd ed., CRC Press, Boca Raton, 2014. https://doi.org/10.1201/b18110

[13] Mehta, P. K., and Monteiro, P. J. M., Concrete: Microstructure, Properties, and Materials, 4th ed., McGraw-Hill Education, New York, 2014.

[14] Neville, A. M., Properties of Concrete, 5th ed., Pearson Education, Harlow, 2011.

[15] ACI Committee 222, Protection of Metals in Concrete Against Corrosion, ACI 222R-19, American Concrete Institute, Farmington Hills, MI, 2019.

[16] ASTM International, ASTM C39/C39M: Standard Test Method for Compressive Strength of Cylindrical Concrete Specimens, ASTM International, West Conshohocken, PA.

[17] ASTM International, ASTM C1556: Standard Test Method for Determining the Apparent Chloride Diffusion Coefficient of Cementitious Mixtures by Bulk Diffusion, ASTM International, West Conshohocken, PA.

[18] EN 12390-12, Testing Hardened Concrete - Part 12: Determination of the Carbonation Resistance of Concrete - Accelerated Carbonation Method, European Committee for Standardization, Brussels, 2020.

[19] Bernal, S. A., Dhandapani, Y., Elakneswaran, Y., et al., Report of RILEM TC 281-CCC: A critical review of the standardised testing methods to determine carbonation resistance of concrete, Materials and Structures, Vol. 57, Article 173, 2024. https://doi.org/10.1617/s11527-024-02424-9

[20] Abd El-Fattah, H., Abd El-Zaher, Y., and Kohail, M., A study of chloride binding capacity of concrete containing supplementary cementitious materials, Scientific Reports, Vol. 14, Article 12970, 2024. https://doi.org/10.1038/s41598-024-62778-6

[21] Georget, F., Babaahmadi, A., Machner, A., et al., Measuring chloride binding in cementitious materials: A review by RILEM TC 298-EBD, Materials and Structures, Vol. 58, Article 348, 2025. https://doi.org/10.1617/s11527-025-02802-x

[22] De Weerdt, K., Chloride binding in concrete: Recent investigations and recognised knowledge gaps, Materials and Structures, Vol. 54, Article 214, 2021. https://doi.org/10.1617/s11527-021-01793-9

[23] Sui, S., Wilson, W., Georget, F., Maraghechi, H., Kazemi-Kamyab, H., Sun, W., and Scrivener, K., Quantification methods for chloride binding in Portland cement and limestone systems, Cement and Concrete Research, Vol. 125, 105864, 2019. https://doi.org/10.1016/j.cemconres.2019.105864

[24] Babaahmadi, A., Machner, A., Kunther, W., Figueira, J., Hemstad, P., and De Weerdt, K., Chloride binding in Portland composite cements containing metakaolin and silica fume, Cement and Concrete Research, Vol. 161, 106924, 2022. https://doi.org/10.1016/j.cemconres.2022.106924